

The Long-term Radiative Evolution of Anomalous X-ray Pulsar 1E 2259+586 after its 2002 Outburst

Weiwei Zhu¹, Victoria M. Kaspi^{1,2}, Rim Dib¹, Peter M. Woods^{3,4}, Fotis P. Gavriil^{5,6} and
Anne M. Archibald¹

ABSTRACT

We present an analysis of five X-ray Multi-Mirror Mission (*XMM*) observations of the anomalous X-ray pulsar (AXP) 1E 2259+586 taken in 2004 and 2005 during its relaxation following its 2002 outburst. We compare these data with those of five previous *XMM* observations taken in 2002 and 2003, and find the observed flux decay is well described by a power law of index -0.69 ± 0.03 . As of mid-2005, the source may still have been brighter than preoutburst, and was certainly hotter. We find a strong correlation between hardness and flux, as seen in other AXPs. We discuss the implications of these results for the magnetar model.

Subject headings: pulsars: individual (1E 2259+586) — X-rays: stars — stars: neutron

1. Introduction

It is now commonly believed that soft gamma-ray repeaters (SGRs) and anomalous X-ray pulsars (AXPs) are neutron stars with ultra-strong magnetic fields, i.e. magnetars (Duncan & Thompson 1992). Their common nature was conclusively demonstrated when

¹Department of Physics, McGill University, Montreal, QC, H3A 2T8, Canada; zhuww@physics.mcgill.ca, vkaspi@physics.mcgill.ca, rim@physics.mcgill.ca, aarchiba@physics.mcgill.ca

²Canada Research Chair; Lorne Trottier Chair; R. Howard Webster Fellow of CIFAR

³Dynetics, Inc., 1000 Explorer Boulevard, Huntsville, AL, 35806

⁴NSSTC, 320 Sparkman Drive, Huntsville, AL, 35805

⁵NASA Goddard Space Flight Center, Astrophysics Science Division, Code 662, Greenbelt, MD, 20771

⁶Center for Research and Exploration in Space Science and Technology, University of Maryland Baltimore County, 1000 Hilltop Circle, Baltimore, MD 21250

AXP 1E 1048.1–5937 was observed to emit SGR-like bursts in 2001 (Gavriil et al. 2002) and 1E 2259+586, in the supernova remnant (SNR) CTB 109, was seen to undergo a major SGR-like outburst in 2002 (Kaspi et al. 2003; Woods et al. 2004). Subsequently, a variety of different types of activity in AXPs have been seen, including short- and long-term flux variations (Gavriil & Kaspi 2004; Dib et al. 2007) and slow and rapid pulse profile changes (Iwasawa et al. 1992; Kaspi et al. 2003; Woods et al. 2004; Israel et al. 2007; Dib et al. 2007, 2008), in addition to bursts and outbursts (Gavriil et al. 2006; Woods et al. 2005; Dib et al. 2007; see Kaspi 2007 for a recent review).

During 1E 2259+586’s 2002 outburst, the pulsed and persistent fluxes rose suddenly by a factor of ≥ 20 and decayed on a timescale of months. Coincident with the X-ray brightening, the pulsar suffered a large glitch of fractional frequency change 4×10^{-6} (Kaspi et al. 2003; Woods et al. 2004). In the first few hours of the outburst, the pulsar’s pulse profile changed significantly, its pulsed fraction decreased, and its spectrum hardened dramatically. Over 80 short SGR-like bursts from the pulsar were observed at the same time (Gavriil et al. 2004). A near-infrared (K_s) enhancement was also observed during the epoch of the outburst (Kaspi et al. 2003).

Combining *Rossi X-Ray Timing Explorer* (*RXTE*) observations and *XMM* observations of 1E 2259+586 taken during and after the outburst, Woods et al. (2004) found that the decay of 1E 2259+586’s unabsorbed flux (mostly inferred from *RXTE* pulsed fluxes) after the outburst was well characterized by two power law components: a rapid steep decay visible only during the first several hours (< 1 day) of the outburst, and a slower decay of index -0.22 for the next several months. Tam et al. (2004) found that the near-infrared enhancement at late times decayed at the same rate as the slow X-ray decay, although there were no IR observations during the first few hours of the outburst.

Other AXPs have also exhibited transient behavior that could be explained by SGR-like outbursts. AXP XTE J1810–197 is called transient because it was only discovered in 2003 when it suddenly became brighter by a factor of 100 (Ibrahim et al. 2004; Gotthelf et al. 2004). Gotthelf & Halpern (2007) found that the flux of XTE J1810–197 after 2003 followed an exponential decay of timescale 233.5 days. Similarly, the AXP CXOU J164710.2–455216 was found to have brightened by a factor of ~ 300 between two *XMM* observations taken 5 days apart in 2006 September (Israel et al. 2007). Candidate AXP AX 1845–0258, was discovered in an observation made in 1993 by *ASCA* (Gotthelf & Vasisht 1998; Torii et al. 1998). Follow-up observations in 1999 showed that the source’s flux was smaller by a factor of ~ 10 (Vasisht et al. 2000). Tam et al. (2006) found that AX 1845–0258 remains undetected in *Chandra* observations taken in 2003, with its flux ~ 260 -430 times fainter than observed in 1993.

The transient AXP phenomena summarized above are qualitatively similar to the 1998 August 27 flare of SGR 1900+14, in which the X-ray flux decayed with a power law of index ~ -0.9 (Feroci et al. 2003), and the flux decay of SGR 1627–41 since 1998, which followed a power law of index ~ -0.47 and lasted for ~ 800 days (Kouveliotou et al. 2003). However, thus far, the AXP outbursts have been much less energetic than most SGR outbursts. Also, most of the burst energy was released during the afterglows of the AXP outbursts, while for SGR outbursts, the X-ray afterglows have less integrated energy than the burst itself.

With now a handful of AXP and SGR outbursts and subsequent relaxations observed, we can begin to look for correlations between different outburst and relaxation properties in the hope of constraining magnetar physics. For example, SGR outburst recoveries have been modeled as crustal cooling following impulsive heat injection, and in principle can yield constraints on the nature of the crustal matter (Lyubarsky et al. 2002). Alternatively, the AXP events have been interpreted in terms of magnetospheric twisting (Thompson et al. 2002; Beloborodov & Thompson 2007), whose recovery depends on electrodynamics in the region of the magnetosphere immediately outside the stellar surface. On the other hand, Güver et al. (2007) suggest that AXP recoveries can be modeled with a stationary magnetosphere, with only the surface temperature changing. They argue that their model, which includes the stellar atmosphere, can be used to quantitatively determine the source’s magnetic field.

In this paper we present a spectral and pulsed flux analysis of 10 *XMM* observations of AXP 1E 2259+586 taken between 2002 and 2005, as the source relaxed back toward quiescence following its 2002 outburst. We compare the X-ray flux and spectral evolution of 1E 2259+586 with those of other magnetars, and interpret these results in terms of the magnetar model.

2. Observations

2.1. *XMM*-Newton Observations

Ten *XMM* (Jansen et al. 2001) observations were analyzed for this paper. The first five observations of 1E 2259+586 were taken between 2002 and 2003, just prior to and after the 2002 June outburst. Data from these five observations have already been presented in Woods et al. (2004). We re-analyzed these observations using the *XMM* calibrations published on 2007 September 4 (*XMM*-CCF-REL-239¹). The later five observations were taken

¹See http://xmm.esac.esa.int/external/xmm_sw_cal/calib/rel_notes/index.shtml

between 2004 and 2005. Most of these observations pointed at 1E 2259+586, with the European Photon Imaging Camera (EPIC) pn camera (Strüder et al. 2001) in Small Window Mode. However, three observations were obtained with *XMM* pointing at a portion of the SNR CTB 109’s shell and with the pn camera in extended Full Frame Mode. Details about the observational modes, pointing offsets, and exposure times are presented in Table 1. The EPIC mos cameras (Turner et al. 2001) were operating in Full window mode with the medium filter in four of the first five observations, the exception being the third, and therefore the observed spectra are highly piled-up. The mos cameras were operated in Small Window Mode with the thick filter in the remaining observations, and hence with lower efficiency than for the pn camera. Nevertheless, we analyzed the mos data and found the resulting fluxes and parameters were quantitatively in agreement with those from pn data, given the current knowledge of cross-calibration uncertainties between the two instruments.² In this paper we report only the higher quality EPIC pn data.

The data were analyzed with the *XMM* Science Analysis System (SAS) version 7.1.0³ and the latest calibrations. Strong background flares can sometimes contaminate source events. To exclude possible flares, we extracted light curves from the entire field of view for events having energy > 10 keV. We then examined these light curves for flares. We defined bad time intervals to be when flares occurred, and excluded these intervals for all subsequent analyses. For all the *XMM* observations, we filtered a total of 20 ks of bad time intervals. Then we corrected the event times to the barycenter using the SAS `barycen` tool.

2.2. *RXTE* observations

We have observed AXP 1E 2259+586 regularly since 1997 with *RXTE* (see, e.g., Gavriil & Kaspi 2002). Our data were obtained using the Proportional Counter Array (PCA) on board *RXTE* (Jahoda et al. 2006). The PCA consists of five identical and independent xenon/methane Proportional Counter Units (PCUs). We use our *RXTE* observations of 1E 2259+586 to monitor its pulsed flux, and its frequency evolution using phase-coherent timing, and to look for bursts and pulse profile changes.

For the purposes of this paper we analysed 193 observations that took place between 2001 April 1 (MJD 52,000) and 2006 September 22 (MJD 54,000): 15 preoutburst observations, 1 observation during the outburst, and 177 postoutburst observations. All 193 observations

²See <http://xmm.esac.esa.int/docs/documents/CAL-TN-0018-2-6.pdf>, on the current calibration status of the EPIC cameras.

³See <http://xmm.esac.esa.int/sas/7.1.0/>

with the exception of the two observations immediately following the outburst were taken in `GoodXenonwithPropane` or `GoodXenon` data modes. Both data modes record photon arrival times with $1 \mu\text{s}$ resolution and bin photon energies into one of 256 channels. To maximize the signal-to-noise ratio, we analysed only those events from the top xenon layer of each PCU. The remaining two observations were in event modes with a time resolution of $\sim 125 \mu\text{s}$, a smaller number of energy channels, and no possibility of layer selection. For each of the observations we created barycentered light curves in the 2–10 keV band with 31.25 ms time resolution.

We then folded each of the light curves using an ephemeris determined iteratively by maintaining phase coherence (see, e.g., Gavriil & Kaspi 2002). We then used the folded profiles to calculate the pulsed flux for each observation using both an rms estimator (see, e.g., Woods et al. 2004) and an area estimator after baseline subtraction (see Archibald et al. 2008 in preparation, for details). The results obtained using the two methods were consistent with each other. Here we only report the area pulsed flux because, while more sensitive to noise, it is the quantity of primary interest.

To calculate the area pulsed flux for a given folded time series, we used the following:

$$PF_{area} = \sum_{i=1}^N (p_i - p_{min})/N, \quad (1)$$

where p_i refers to the count rate in the i th bin, N is the number of phase bins, and p_{min} is the average count rate in the off-pulse phase of the profile, determined by cross-correlating with a high signal-to-noise ratio template, and calculated in the Fourier domain after truncating the Fourier series to six harmonics. Finally, we combined the pulsed flux numbers from each of two consecutive weeks into a single number, with the exception of the burst observation and the two observations that followed it, which remained unbinned. The results are presented in Figure 1a.

3. Analysis and Results

3.1. Spectrum evolution

Source spectra were extracted from circular regions of $32''.5$ radius around the source center, using the barycentered, filtered event file described in §2.1. Background spectra were extracted from circular regions of $50''$ radius centered $\sim 3'$ away from the source center. For the observations taken in Small Window Mode, we extracted single- and double-photon events and excluded events on or close to a bad pixel using the filter expression “FLAG

= 0 && PATTERN <= 4". In the Full Frame Mode observations, the source is highly off-center in the CCD image (Table 1), and bad pixels were found close to the source center region. For these observations, the event list was filtered using the selection expression #XMMEA_EP to exclude only photons which fall directly on the bad pixels. However, we did not exclude photon events located adjacent to the bad pixel (which normally would be excluded by the expression FLAG = 0), because when there is a bad pixel close to the center of the source region, the effective area is evaluated more accurately with pixels around the bad ones taken into account by the SAS command `arfgen` (*XMM* help desk 2008, private communication). In order to avoid events that affected multiple pixels, we used only single events (PATTERN= 0) in the Full Frame Mode data. Event lists thus extracted were input to `ftool grppha`, which grouped the events by at least 25 photons per bin. A systematic uncertainty of 2% was also appended to the output spectra using `grppha` in order to characterize the current level of calibration accuracy.⁴

The resultant spectra were fitted in XSPEC 12.3.0⁵ with the commonly used photoelectrically absorbed blackbody plus power law model in the energy range 0.6–12 keV. Because the hydrogen column density N_H is not expected to be variable, we fixed this parameter for all the data sets and performed a joint fit. The goodness of fit is reasonable (see χ^2_ν in Table 2). The best-fit N_H is $(1.012 \pm 0.007) \times 10^{22} \text{ cm}^{-2}$.

This value is consistent with that estimated from fitting individual absorption edges of elements O, Fe, Ne, Mg, and Si in the *XMM* RGS spectra (Durant & van Kerkwijk 2006). The other parameters were set free to vary and their best-fit values are presented in Table 2. The best-fit blackbody temperature, blackbody radius, and power law index are plotted versus time in Figure 1.

In order to look for correlations between spectral hardness and flux as observed in other AXPs (Rea et al. 2005; Campana et al. 2007; Tam et al. 2008b; Gonzalez et al. 2008), we have looked for a correlation between hardness ratio and observed flux. We define the hardness ratio to be the ratio of 2–10 keV absorbed flux to 0.1–2 keV absorbed flux. We find the hardness ratio to be strongly correlated with the 2–10 keV absorbed flux (as shown in Fig. 2a) in our observations. An anti-correlation between photon index and 2–10 keV unabsorbed flux is also seen, but has more scatter (as shown in Fig. 2b). This is likely because the photon index is not a perfect measure of spectral hardness, as it can be strongly influenced by the spectral fit at the low end of the band.

⁴See <http://xmm.esac.esa.int/docs/documents/CAL-TN-0018.pdf>, (*EPIC Status of Calibration and Data Analysis*)

⁵See <http://heasarc.gsfc.nasa.gov/docs/xanadu/xspec/>

3.2. Pulsed fractions

We folded the 0.1–2 and 2–10 keV light curves of each *XMM* observation at the pulsar’s period, determined using an ephemeris derived by phase coherent timing, from *RXTE* monitoring (Table 1; see Dib et al. 2007 for details). Each pulse profile was constructed by folding the photons into 32 phase bins. We measured area pulsed flux of the *XMM* the same way we did for *RXTE* (see eq.1), except that we used eight harmonics instead of six when smoothing the light curves (for details see Archibald et al. 2008 in preparation).

The measured area pulsed fractions are plotted in Figure 1*f*. A possible correlation between the 0.1–2 keV area pulsed fraction and the 2–10 keV unabsorbed flux is seen (Fig. 3, *filled circles*). A similar correlation was also found between the 0.1–2 keV area pulsed fraction and the 0.1–2 keV absorbed flux. However, the correlation between 2–10 keV pulsed fraction and flux is not significant (Fig. 3, *open boxes*).

We also measured the rms pulsed fraction from the profiles to compare with the area pulsed fraction results. The 2–10 keV rms pulsed fractions are consistent with being constant, while the 0.1–2 keV rms pulsed fractions have some variance, but no significant trend or correlation with other parameters. The area and rms pulsed fractions are different by a factor that depends on the shape of the profile; as the pulse profile of 1E 2259+586 did change temporarily after the outburst (from a simple double peaked profile to triple peaked; Kaspi et al. 2003; Woods et al. 2004), the different result is not surprising.

3.3. Flux evolution

We fit the unabsorbed fluxes measured in our *XMM* observations after the outburst with a power law plus constant decay model, $F(t) = F_b[(t - t_g)/(1 \text{ day})]^\alpha + F_q$, where $F(t)$ denotes the unabsorbed flux, F_b is the unabsorbed source flux one day after the onset of the outburst, F_q is the quiescent flux and t_g marks the glitch epoch MJD 52,443.13 (Woods et al. 2004). A good fit of $\chi_\nu^2(\nu) = 0.66(5)$ (Fig. 4, *dashed line*) was found. The best-fit power law index $\alpha = -0.69 \pm 0.03$ (Table 3). The quiescent flux level we found from this power law fit is $(1.75 \pm 0.02) \times 10^{-11} \text{ ergs s}^{-1} \text{ cm}^{-2}$, considerably higher than that measured one week before the outburst $[(1.59 \pm 0.01) \times 10^{-11} \text{ ergs s}^{-1} \text{ cm}^{-2}$; Table 2]. We also fit the *XMM* unabsorbed fluxes with an exponential decay plus quiescent level model, $F(t) = F_p e^{-(t-t_g)/\tau} + F_q$, where $F(t)$ is unabsorbed flux, F_p is the peak flux, F_q is the quiescent flux, τ is the decay timescale and t_g marks the glitch epoch. The fit is worse than that of the power law decay model but still acceptable, with $\chi_\nu^2(\nu)$ of 1.08(5). The best-fit decay timescale τ is 13.3 ± 0.7 days. Best-fit flux decay parameters are presented in Table 3.

We also fit power law and exponential models to the area pulsed flux of 1E 2259+586 measured by *RXTE* from 12 to 1649 days after the glitch. A power law model fits the data much better than the exponential model [$\chi^2_\nu(\nu) = 1.18(69)$ for the power law model, $\chi^2_\nu(\nu) = 1.65(69)$ for the exponential decay model; Table 3], which is evidence against the latter. The best-fit exponential decay timescale for *RXTE* data is 134 ± 15 days, an order of magnitude different from the ~ 13 day timescale found for the *XMM* data.

The best-fit power law plus constant model for the evolution of the *RXTE* pulsed fluxes is different from that of the *XMM* total fluxes. This suggests that the 2–10 keV pulsed fractions were varying. In principle, we can check this with the pulsed fraction measurements we made with *XMM* (see § 3.2). Given the uncertainties on the *XMM* 2–10 keV pulsed fractions (Table 2), as well as those of the best-fit evolution models (Table 3), we find that the two are in agreement.

Gotthelf & Halpern (2007) fit the spectrum of XTE J1810–197 using a double-blackbody model when studying that source’s relaxation following its outburst. In order to compare the spectrum and evolution of 1E 2259+586 to that of XTE J1810–197, we also fit a photoelectrically absorbed double-blackbody model to 1E 2259+586’s spectra jointly. A double-blackbody model does not fit the spectra as well as the blackbody plus power law model (see Table 2 for details). The best-fit N_H for the double-blackbody model [$(0.568 \pm 0.03) \times 10^{22} \text{ cm}^{-2}$] is smaller than that from our blackbody plus power law fit and is not consistent with the value measured independently from RGS spectra [$(1.12 \pm 0.33) \times 10^{22} \text{ cm}^{-2}$; Durant & van Kerkwijk 2006], but is consistent with the best-fit N_H [$(0.5\text{--}0.7) \times 10^{22} \text{ cm}^{-2}$] of CTB 109 measured by Sasaki et al. (2004).

Unabsorbed fluxes obtained using the double-blackbody spectral model can also be fitted to a power law decay or an exponential decay model. The best-fit power law index is -0.73 ± 0.04 , and the best-fit exponential timescale is 12.7 ± 0.7 days (Table 3), consistent with what we obtained using the blackbody plus power law spectral model. This indicates that our results for the decay parameters are independent of the choice of spectral model. In the analysis of XTE J1810–197 by Gotthelf & Halpern (2007), they found that both of the two-blackbody components’ flux followed an exponential decay after XTE J1810–197’s 2003 outburst. However, we find that the flux of 1E 2259+586’s soft blackbody component measured from our fourth and fifth observations (only ~ 21 days after the outburst and glitch) were lower than that measured for the last five observations (see Table 2 for details). This flux variation of the soft blackbody component therefore cannot be well fitted with an exponential or power law decay model. The temperatures of both the hotter and cooler components were also lower in the fourth and fifth observations than in the last five observations. The non-monotonic variation of the soft blackbody flux and the two components’ temperature are

different from what was observed by Gotthelf & Halpern (2007) and suggest that the double-blackbody model is not a reasonable representation of the spectrum of 1E 2259+586. On the other hand, the spectral evolution from the blackbody plus power law spectral fit looks more reasonable. Using this spectral model, the blackbody radius in the first postoutburst observation was small compared to that of the preoutburst observations and was even smaller in the second and third postoutburst observations (Fig. 1*d*), suggesting that one or more hot spots formed after the outburst and were fading away in the next few months. In the last five observations, the blackbody radius was as large as the preoutburst value, suggesting that the putative hot spots had completely faded away and the thermal radiation then mostly came from the bulk surface of the neutron star as it did before outburst. Perhaps a more realistic spectral model such as that of Güver et al. (2007, 2008) could describe the spectral evolution of 1E 2259+586 better, but such an analysis is outside the scope of this paper.

Based on *RXTE* observations, Woods et al. (2004) found that the decay of 1E 2259+586’s 2002 outburst consisted of two parts: a steeper power law decay in the first few hours, and a slower power law decay afterwards. They also found that the total energy released (2–10 keV) in the slower decay was 2.1×10^{41} ergs, which is much larger than the total energy (2–60 keV) released in the bursts (6×10^{37} ergs; Gavriil et al. 2004). We also studied the slower decay, by fitting a power law plus constant model, instead of the simple power law model used by Woods et al. (2004). The total released energy, according to our best-fit model, is roughly consistent with that calculated by Woods et al. (2004): we find $\simeq 3 \times 10^{41}$ ergs (2–10 keV), assuming that the outburst will be over in 10000 days. However, based on our best-fit exponential model, the total energy released was somewhat smaller, $\simeq (3 - 4) \times 10^{40}$ ergs (2–10 keV).

4. Discussion

In this paper, we have presented a comprehensive study of the X-ray recovery of AXP 1E 2259+586 following its 2002 outburst. Here we discuss the properties of this recovery, compare them with those of other magnetar outbursts, and consider how they constrain the magnetar model.

4.1. Return to “Quiescence”

In our 2004 and 2005 *XMM* observations, the source’s temperature and unabsorbed fluxes were still higher than the preoutburst value (Fig. 1). This suggests that the source

was not fully back to the preoutburst flux level. Our power law fit to the flux decay shows that the after-outburst quiescent flux level is $(1.75 \pm 0.02) \times 10^{-11}$ ergs s $^{-1}$ cm $^{-2}$, which is significantly higher than the preoutburst value [$(1.59 \pm 0.01) \times 10^{-11}$ ergs s $^{-1}$ cm $^{-2}$; Table 3]. Either the 2005 flux had still not returned to its quiescent level, or perhaps it had returned to quiescence but the flux just before the event was unusually low. Also possible is that this (and other) AXPs do not have well-defined constant quiescent fluxes, but have long-term flux variations. Indeed, there is evidence for some X-ray flux variability in 1E 2259+586 over the years since its discovery in 1981 (Baykal & Swank 1996). Other AXPs also show variability on a variety of timescales (see Kaspi 2007 for a review).

4.2. Comparison with other Magnetar Recoveries

It is useful to compare the behavior observed from 1E 2259+586 with that of other magnetars. SGR 1900+14’s flux was found to follow a power law of index -0.713 ± 0.025 after its 1998 August 27 flare (Woods et al. 2001).⁶ This has been interpreted as the cooling of the magnetar outer crust following a sudden release of magnetic energy (Lyubarsky et al. 2002). This model predicts a power law decay of index $\sim -2/3$. The flux of SGR 1627–41 was found to decay following a power law of index ~ -0.47 since its 1998 source activation. Approximately 800 days after the source activation, SGR 1627–41’s flux suddenly declined by a factor of 10. This behavior is also well fitted by the crust cooling model, although with some fine tuning (Kouveliotou et al. 2003). We fit the *XMM* 2–10 keV unabsorbed fluxes of 1E 2259+586 with a power law plus constant model, and found the best-fit power law index to be -0.69 ± 0.03 , close to that of SGR 1900+14, and that predicted by the model. This suggests that the 1E 2259+586 outburst afterglow may also be explained by the diffusion of heat in the outer crust.

The transient AXP XTE J1810–197 exhibited an outburst in 2003. Ibrahim et al. (2004) found that the afterglow of the XTE J1810–197 outburst as observed by *RXTE* could be described by a power law decay model ($F \propto t^{-\beta}$) with $\beta = 0.45 - 0.73$. This is similar to the behavior of 1E 2259+586 and other SGRs. However, Gotthelf & Halpern (2007) found that, with more observations taken by *Chandra* from 2003 to 2006, the afterglow of the XTE J1810–197 outburst actually followed an exponential decay of timescale 233.5 days. As we have shown in this paper, the pulsed and unabsorbed X-ray flux decay of 1E 2259+586

⁶Later the afterglow of the SGR 1900+14 August 27 flare was fitted with a power law plus constant model instead of the single power law model used by Woods et al. (2001), and a decay index of ~ 0.9 was obtained (Feroci et al. 2003).

favors the power law decay model over the exponential decay. Perhaps the physical processes involved in the 2003 outburst of XTE J1810–197 were different from those in 2002 outburst of 1E 2259+586.

4.3. Twisted Magnetosphere Model

Thompson et al. (2002) reported that, if there exists a global twist of the magnetosphere, the decay timescale τ of this twist would be

$$\tau = 40\Delta\phi^2\left(\frac{L_X}{10^{35}\text{ergs s}^{-1}}\right)^{-1}\left(\frac{B_{\text{pole}}}{10^{14}\text{G}}\right)^2\left(\frac{R_{\text{NS}}}{10\text{km}}\right)^3\text{yr}. \quad (2)$$

Woods et al. (2004) argued that, for 1E 2259+586, the twist angle $\Delta\phi$ should be $\sim 10^{-2}$ rad. Thus, the predicted twist relaxation timescale of 1E 2259+586 is several hours, which is coincidentally the timescale of the steeper flux decay observed at the beginning of the afterglow.

However, Beloborodov & Thompson (2007) have shown more recently that this decay timescale is actually expected to be much larger than equation (2) suggests. This is because, in their model, the self-induction of the twisted portion of the magnetosphere accelerates particles from the stellar surface and initiates avalanches of pair creation which forms the corona. This corona persists in dynamic equilibrium, maintaining the electric current, as long as dissipation permits. The relevant timescale in this picture for the decay of a sudden twist is given by

$$\tau \simeq 0.3\left(\frac{L_X}{10^{35}\text{ergs s}^{-1}}\right)\left(\frac{e\Phi_e}{\text{GeV}}\right)^{-2}\left(\frac{R_{\text{NS}}}{10\text{km}}\right)\text{yr}, \quad (3)$$

where L_X is the peak X-ray luminosity and $e\Phi_e$ is the voltage along the twisted magnetic field lines and should nearly universally be ~ 1 GeV (see Beloborodov & Thompson 2007). For 1E 2259+586, we find $\tau \simeq 1.2$ yr, given the peak luminosity $L_X \sim 4 \times 10^{35}(d/3 \text{ kpc}) \text{ ergs s}^{-1}$. Thus, the longer observed decay after the initial steep decline may indeed correspond to the untwisting of a coronal flux tube in the Beloborodov & Thompson (2007) picture, although the predicted timescale is somewhat smaller than the observed time to return to quiescence. We note that the Beloborodov & Thompson (2007) model predicts a linear flux decline, in contrast to what we have observed for 1E 2259+586 and what has been observed for XTE J1810–197 (Gotthelf & Halpern 2007). Moreover, in the ~ 5 yr of *RXTE* monitoring of 1E 2259+586 prior to its 2002 outburst (Gavriil & Kaspi 2002), its pulsed X-ray luminosity in the 2–10 keV band was roughly constant at $\sim 2 \times 10^{34} \text{ ergs s}^{-1}$. This also is puzzling given the Beloborodov & Thompson (2007) prediction that if the time between large-scale events is longer than the decay time from the previous event, the magnetar should enter a quiescent

state in which the observed luminosity is dominated by the surface blackbody emission. Why should the “quiescent” blackbody emission from 1E 2259+586 be a full order of magnitude larger than that from XTE J1810–197, especially given the latter’s much larger inferred magnetic field (1.7×10^{14} versus 6×10^{13} G)? This disparity in “quiescent,” steady luminosities is even larger when considering AXP 1E 1841–045, which has an apparently steady 2–10 keV luminosity of 1.4×10^{35} ergs s^{-1} , and comparing with probable AXP AX 1845–0258, which has quiescent luminosity approximately 2 orders of magnitude smaller (Tam et al. 2006). Distance uncertainties may contribute but not on a scale that can significantly alleviate this problem. This remains an interesting puzzle in magnetar physics.

The twisted magnetosphere or flux tube models generically predict that the flux and spectral hardness of magnetars in outburst should be roughly correlated due to increased scattering optical depth when the twist is larger. However, a similar prediction for a flux/hardness correlation was made by Özel & Güver (2007) in their thermally emitting magnetar model, using a simple prescription for the magnetosphere and scattering geometry, with the latter stationary, i.e. invoking no variable magnetospheric twists. Güver et al. (2007) found that their model could reproduce the existing data for XTE J1810–197. We note that hardness-intensity correlations have now been observed for RXS J170849.0–400910 (Campana et al. 2007), 1E 1048.1–5937 (Tam et al. 2008b), and as we report, in our 1E 2259+586 *XMM* observations. It would be interesting to apply analysis of Özel & Güver (2007) to these data, but it is outside the scope of this paper.

4.4. Other Observed Recovery Properties

The fact that the rms and area pulsed fractions remained largely constant while the blackbody radius (in the blackbody plus power law model) changed by a factor of ~ 2 (Fig. 1) is worth considering, if the empirical blackbody plus power law spectrum model somehow resembles the real radiation mechanism. Pulsed fraction should generally decrease when the thermally radiating region on the star grows, provided that this region is not very small compared to the entire surface. Any realistic spectral model which takes radiative transfer in the atmosphere and scattering through the magnetosphere into account should be able to reproduce the observation in this regard as well.

A clear anti-correlation between 1E 1048.1–5937’s pulsed fraction and unabsorbed flux has been observed (Tiengo et al. 2005; Gavriil et al. 2006; Tam et al. 2008b). However, we found no such correlation in the 2–10 keV band for 1E 2259+586. On the contrary, its 0.1–2 keV area pulsed fractions seem to be correlated with both 0.1–2 and 2–10 keV unabsorbed fluxes (see Fig. 3). Gotthelf & Halpern (2007) found that XTE J1810–197’s pulsed fraction

measured between 2003 and 2006 after its outburst decreased with the decay of its flux, i.e. XTE J1810–197’s pulsed fraction is also correlated with flux. Thus, the striking anti-correlation between pulsed fraction and flux observed from 1E 1048.1–5937 is clearly not universal.

Finally, we note that the near-infrared flux decay of 1E 2259+586 was found to follow a power law of index $-0.75_{-0.33}^{+0.22}$ when fitted to a power law plus constant model (Tam et al. 2004). This decay index is close to what we found for the X-ray flux decay, thus confirming the reported correlation between near-IR and X-ray fluxes postoutburst.⁷ Tam et al. (2008a) and Wang et al. (2008) showed that the near-IR flux of 1E 1048.1–5937 do show correlation with X-rays at times of outbursts. However, Camilo et al. (2007) show that the near-IR flux variation of XTE J1810–197 is not simply correlated with X-ray flux nor even monotonic postoutburst. Thus, the AXP picture with regard to near-IR variability is not yet fully clear.

We thank A. Beloborodov, A. Cumming, and G. Vasisht for useful discussions. Support for this work was provided by an NSERC Discovery grant Rgpin 228738-03, an R. Howard Webster Fellowship of the Canadian Institute for Advanced Research, Les Fonds de la Recherche sur la Nature et les Technologies, a Canada Research Chair, and the Lorne Trottier Chair in Astrophysics and Cosmology to VMK. RD was supported by an NSERC PGSD scholarship.

REFERENCES

- Archibald, A. M., Dib, R., & Kaspi, V. M. 2008, in preparation
- Baykal, A. & Swank, J. 1996, *ApJ*, 460, 470
- Beloborodov, A. M. & Thompson, C. 2007, *ApJ*, 657, 967
- Camilo, F., Ransom, S. M., Peñalver, J., Karastergiou, A., van Kerkwijk, M. H., Durant, M., Halpern, J. P., Reynolds, J., Thum, C., Helfand, D. J., Zimmerman, N., & Cognard, I. 2007, *ApJ*, 669, 561
- Campana, S., Rea, N., Israel, G. L., Turolla, R., & Zane, S. 2007, *A&A*, 463, 1047

⁷The -0.22 X-ray decay index reported by Woods et al. (2004) and the -0.21 near-infrared flux decay index reported by Tam et al. (2004) were obtained from a simple power law fitting, i.e. with no quiescent level included in the fit.

- Dib, R., Kaspi, V. M., & Gavriil, F. P. 2007, *ApJ*, 666, 1152
- . 2008, *ApJ*, 673, 1044
- Duncan, R. C. & Thompson, C. 1992, *ApJ*, 392, L9
- Durant, M. & van Kerkwijk, M. H. 2006, *ApJ*, 650, 1082
- Feroci, M., Mereghetti, S., Woods, P., Kouveliotou, C., Costa, E., Frederiks, D. D., Golenetskii, S. V., Hurley, K., Mazets, E., Soffitta, P., & Tavani, M. 2003, *ApJ*, 596, 470
- Gavriil, F. P. & Kaspi, V. M. 2002, *ApJ*, 567, 1067
- . 2004, *ApJ*, 609, L67
- Gavriil, F. P., Kaspi, V. M., & Woods, P. M. 2002, *Nature*, 419, 142
- . 2004, *ApJ*, 607, 959
- Gavriil, F. P., Kaspi, V. M., & Woods, P. M. 2006, *ApJ*, 641, 418
- Gonzalez, M. E., Dib, R., Kaspi, V. M., Woods, P. M., Tam, C. R., & Gavriil, F. P. 2008, arXiv: astro-ph/0708.2756
- Gotthelf, E. V. & Halpern, J. P. 2007, *Ap&SS*, 308, 79
- Gotthelf, E. V., Halpern, J. P., Buxton, M., & Bailyn, C. 2004, *ApJ*, 605, 368
- Gotthelf, E. V. & Vasisht, G. 1998, *New Astronomy*, 3, 293
- Güver, T., Özel, F., & Göğüş, E. 2008, *ApJ*, 675, 1499
- Güver, T., Özel, F., Göğüş, E., & Kouveliotou, C. 2007, *ApJ*, 667, L73
- Ibrahim, A. I., Markwardt, C. B., Swank, J. H., Ransom, S., Roberts, M., Kaspi, V., Woods, P. M., Safi-Harb, S., Balman, S., Parke, W. C., Kouveliotou, C., Hurley, K., & Cline, T. 2004, *ApJ*, 609, L21
- Israel, G. L., Campana, S., Dall’Osso, S., Munro, M. P., Cummings, J., Perna, R., & Stella, L. 2007, *ApJ*, 664, 448
- Iwasawa, K., Koyama, K., & Halpern, J. P. 1992, *PASJ*, 44, 9
- Jahoda, K., Markwardt, C. B., Radeva, Y., Rots, A. H., Stark, M. J., Swank, J. H., Strohmayer, T. E., & Zhang, W. 2006, *ApJS*, 163, 401

- Jansen, F., Lumb, D., Altieri, B., Clavel, J., Ehle, M., Erd, C., Gabriel, C., Guainazzi, M., Gondoin, P., Much, R., Munoz, R., Santos, M., Schartel, N., Texier, D., & Vacanti, G. 2001, *A&A*, 365, L1
- Kaspi, V. M. 2007, *Ap&SS*, 308, 1
- Kaspi, V. M., Gavriil, F. P., Woods, P. M., Jensen, J. B., Roberts, M. S. E., & Chakrabarty, D. 2003, *ApJ*, 588, L93
- Kothes, R., Uyaniker, B., & Yar, A. 2002, *ApJ*, 576, 169
- Kouveliotou, C., Eichler, D., Woods, P. M., Lyubarsky, Y., Patel, S. K., Göğüş, E., van der Klis, M., Tennant, A., Wachter, S., & Hurley, K. 2003, *ApJ*, 596, L79
- Lyubarsky, Y., Eichler, D., & Thompson, C. 2002, *ApJ*, 580, L69
- Özel, F. & Güver, T. 2007, *ApJ*, 659, L141
- Rea, N., Oosterbroek, T., Zane, S., Turolla, R., Méndez, M., Israel, G. L., Stella, L., & Haberl, F. 2005, *MNRAS*, 361, 710
- Sasaki, M., Plucinsky, P. P., Gaetz, T. J., Smith, R. K., Edgar, R. J., & Slane, P. O. 2004, *ApJ*, 617, 322
- Strüder, L., Briel, U., Dennerl, K., Hartmann, R., Kendziorra, E., Meidinger, N., Pfeffermann, E., Reppin, C., Aschenbach, B., Bornemann, W., Bräuninger, H., Burkert, W., Elender, M., Freyberg, M., Haberl, F., Hartner, G., Heuschmann, F., Hippmann, H., Kastelic, E., Kemmer, S., Kettenring, G., Kink, W., Krause, N., Müller, S., Opitz, A., Pietsch, W., Popp, M., Predehl, P., Read, A., Stephan, K. H., Stötter, D., Trümper, J., Holl, P., Kemmer, J., Soltau, H., Stötter, R., Weber, U., Weichert, U., von Zanthier, C., Carathanassis, D., Lutz, G., Richter, R. H., Solc, P., Böttcher, H., Kuster, M., Staubert, R., Abbey, A., Holland, A., Turner, M., Balasini, M., Bignami, G. F., La Palombara, N., Villa, G., Buttler, W., Gianini, F., Lainé, R., Lumb, D., & Dhez, P. 2001, *A&A*, 365, L18
- Tam, C. R., Gavriil, F. P., Dib, R., Kaspi, V. M., Woods, P. M., & Bassa, C. 2008a, in *American Institute of Physics Conference Series*, Vol. 983, American Institute of Physics Conference Series, 271–273
- Tam, C. R., Gavriil, F. P., Dib, R., Kaspi, V. M., Woods, P. M., & Bassa, C. 2008b, *ApJ*, accepted arXiv:0707.2093
- Tam, C. R., Kaspi, V. M., Gaensler, B. M., & Gotthelf, E. V. 2006, *ApJ*, 652, 548

- Tam, C. R., Kaspi, V. M., van Kerkwijk, M. H., & Durant, M. 2004, *ApJ*, 617, L53
- Thompson, C., Lyutikov, M., & Kulkarni, S. R. 2002, *ApJ*, 574, 332
- Tiengo, A., Mereghetti, S., Turolla, R., Zane, S., Rea, N., Stella, L., & Israel, G. L. 2005, *A&A*, 437, 997
- Torii, K., Kinugasa, K., Katayama, K., Tsunemi, H., & Yamauchi, S. 1998, *ApJ*, 503, 843
- Turner, M. J. L., Abbey, A., Arnaud, M., Balasini, M., Barbera, M., Belsole, E., Bennie, P. J., Bernard, J. P., Bignami, G. F., Boer, M., Briel, U., Butler, I., Cara, C., Chabaud, C., Cole, R., Collura, A., Conte, M., Cros, A., Denby, M., Dhez, P., Di Coco, G., Dowson, J., Ferrando, P., Ghizzardi, S., Gianotti, F., Goodall, C. V., Gretton, L., Griffiths, R. G., Hainaut, O., Hochedez, J. F., Holland, A. D., Jourdain, E., Kendziorra, E., Lagostina, A., Laine, R., La Palombara, N., Lortholary, M., Lumb, D., Marty, P., Molendi, S., Pigot, C., Poindron, E., Pounds, K. A., Reeves, J. N., Reppin, C., Rothenflug, R., Salvétat, P., Sauvageot, J. L., Schmitt, D., Sembay, S., Short, A. D. T., Spragg, J., Stephen, J., Strüder, L., Tiengo, A., Trifoglio, M., Trümper, J., Vercellone, S., Vigroux, L., Villa, G., Ward, M. J., Whitehead, S., & Zonca, E. 2001, *A&A*, 365, L27
- Vasisht, G., Gotthelf, E. V., Torii, K., & Gaensler, B. M. 2000, *ApJ*, 542, L49
- Wang, Z., Bassa, C., Kaspi, V. M., Bryant, J. J., & Morrell, N. 2008, *ApJ*, 679, 1443
- Woods, P. M., Kaspi, V. M., Thompson, C., Gavriil, F. P., Marshall, H. L., Chakrabarty, D., Flanagan, K., Heyl, J., & Hernquist, L. 2004, *ApJ*, 605, 378
- Woods, P. M., Kouveliotou, C., Göğüş, E., Finger, M. H., Swank, J., Smith, D. A., Hurley, K., & Thompson, C. 2001, *ApJ*, 552, 748
- Woods, P. M., Kouveliotou, C., Gavriil, F. P., Kaspi, M. V., Roberts, M. S. E., Ibrahim, A., Markwardt, C. B., Swank, J. H., & Finger, M. H. 2005, *ApJ*, 629, 985

Table 1. *XMM* observation log for 1E 2259+586.

Name	<i>XMM</i> Obsid	Date (MJD TDB)	Date (YY-MM-DD)	pn on-times ^a (ksec)	Off-axis angle (arcmin)	Frequencies ^b (s ⁻¹)
Obs1 ^{cd}	0057540101	52,296.791	02-01-22	8.5	8.7	0.1432871204(7)
Obs2 ^c	0038140101	52,436.413	02-06-11	26.3	2.0	0.143287000(9)
Obs3	0155350301	52,446.446	02-06-21	16.4	2.0	0.14328759(1)
Obs4 ^d	0057540201	52,464.368	02-07-09	5.2	10.7	0.14328754(1)
Obs5 ^d	0057540301	52,464.602	02-07-09	10.2	10.3	0.14328754(1)
Obs6	0203550301	53,055.596	04-02-20	3.6	1.9	0.143286974(7)
Obs7	0203550601	53,162.655	04-06-06	4.8	2.0	0.143286882(4)
Obs8	0203550401	53,178.634	04-06-22	3.4	2.0	0.143286868(2)
Obs9	0203550501	53,358.014	04-12-19	3.5	2.0	0.143286714(1)
Obs10	0203550701	53,579.970	05-07-28	3.3	1.9	0.143286523(7)

^aOn-times quoted reflect on-source times after filtering of background flares.

^bFrequencies are from contemporaneous *RXTE* observations.

^cObservations taken before the outburst, MJD 52,443.13 (Woods et al. 2004).

^dThese three observations were taken in extended Full Frame Mode; all the others were taken in Small Window Mode.

Table 2. 1E 2259+586’s best-fit spectral parameters and pulsed fractions.

Parameter ^{a b}	Obs1	Obs2	Obs3	Obs4	Obs5	Obs6	Obs7	Obs8	Obs9	Obs10
Blackbody plus power law model										
N_H (10^{22} cm ⁻²)	1.012(7)	1.012(7)	1.012(7)	1.012(7)	1.012(7)	1.012(7)	1.012(7)	1.012(7)	1.012(7)	1.012(7)
kT (keV)	0.37(1)	0.406(2)	0.510(4)	0.48(2)	0.49(1)	0.400(7)	0.400(5)	0.400(7)	0.405(7)	0.400(7)
Γ	3.75(4)	3.89(2)	3.49(2)	3.71(5)	3.72(4)	3.77(3)	3.78(3)	3.79(3)	3.79(3)	3.75(3)
Flux ^c	1.15(2)	1.29(1)	3.45(3)	1.95(5)	2.03(4)	1.51(2)	1.48(2)	1.48(2)	1.47(2)	1.45(2)
Unabs Flux ^d	1.41(3)	1.59(1)	4.12(3)	2.34(7)	2.44(5)	1.84(3)	1.82(2)	1.81(3)	1.80(3)	1.77(3)
PL/BB ratio ^e	1.8(3)	1.2(2)	1.6(2)	2.6(4)	2.1(3)	1.6(2)	1.5(2)	1.7(2)	1.5(2)	1.7(2)
Hardness ^f	0.93(3)	0.94(1)	1.43(1)	1.13(4)	1.15(4)	0.98(2)	0.98(2)	0.97(2)	0.98(2)	0.99(2)
χ^2_ν	1.02(5800)		$(P = 0.12)^g$							
Double blackbody model										
N_H (10^{22} cm ⁻²)	0.568(3)	0.568(3)	0.568(3)	0.568(3)	0.568(3)	0.568(3)	0.568(3)	0.568(3)	0.568(3)	0.568(3)
Cooler kT (keV)	0.362(5)	0.372(2)	0.390(3)	0.330(7)	0.335(5)	0.371(3)	0.380(3)	0.371(3)	0.370(4)	0.371(3)
Hotter kT (keV)	0.77(4)	0.82(1)	0.86(1)	0.74(3)	0.73(2)	0.85(3)	0.94(2)	0.89(3)	0.85(3)	0.86(3)
Flux ^c	1.12(6)	1.27(2)	3.34(4)	1.85(9)	1.93(7)	1.48(4)	1.46(3)	1.44(4)	1.44(4)	1.41(4)
Unabs Flux ^d	1.26(6)	1.42(2)	3.69(4)	2.05(11)	2.15(8)	1.65(5)	1.63(4)	1.62(5)	1.61(5)	1.58(5)
HB/CB ratio ^h	0.8(1)	0.6(1)	1.2(2)	2.1(3)	2.0(3)	0.7(1)	0.53(7)	0.64(9)	0.7(1)	0.7(1)
Hardness ^f	0.91(5)	0.92(1)	1.37(2)	1.07(6)	1.09(4)	0.96(3)	0.95(2)	0.94(3)	0.95(3)	0.96(3)
χ^2_ν	1.11(5800)		$(P = 4.6 \times 10^{-9})^g$							
Pulsed fractions										
PF(0.1–2 keV) ⁱ	0.18(3)	0.234(6)	0.322(6)	0.30(2)	0.28(2)	0.29(2)	0.26(1)	0.24(2)	0.27(2)	0.26(2)
PF(2–10 keV) ⁱ	0.23(5)	0.30(1)	0.339(9)	0.33(4)	0.36(3)	0.30(3)	0.33(2)	0.34(3)	0.31(2)	0.29(3)

^aNumbers in parentheses indicate the 1σ uncertainty in the least significant digit. Note that these uncertainties reflect the 1σ error for a reduced χ^2 of unity.

^bBest-fit parameters from a joint fit to all data sets. N_H in all data sets was set to be the same; other parameters were allowed to vary from observation to observation.

^c(10^{-11} ergs s⁻¹cm⁻²). Observed flux from both spectral components in the range 2–10 keV.

^d(10^{-11} ergs s⁻¹cm⁻²). Unabsorbed flux from both spectral components in the range 2–10 keV.

^eThe ratio of power law flux to blackbody flux in the 2–10 keV band (corrected for absorption).

^fSpectral hardness defined as the ratio of 2–10 keV absorbed flux to 0.1–2 keV absorbed flux.

^gThe probability for the χ^2_ν to be higher than that was observed, assuming the model is correct.

^hThe ratio of hot blackbody flux to cool blackbody flux in the 2–10 keV band (corrected for absorption).

ⁱThe area pulsed fractions.

Table 3. Best-fit parameters for the 1E 2259+586 flux decay

Power law decay ^a	$F_q(10^{-11}\text{ergs s}^{-1}\text{cm}^{-2})$	$F_b(10^{-11}\text{ergs s}^{-1}\text{cm}^{-2})$	α	χ^2	χ^2/ν
<i>XMM</i> UF (BB+PL) ^b	(1.75 ± 0.02)	(5.40 ± 0.21)	-0.69 ± 0.03	3.31	0.66
<i>XMM</i> UF (BB+BB) ^c	(1.58 ± 0.01)	(5.07 ± 0.22)	-0.73 ± 0.04	1.22	0.24
<i>RXTE</i> PF ^d	$(0.14 \pm 0.06)\text{cts s}^{-1}\text{PCU}^{-1}$	$(1.4 \pm 0.1)\text{cts s}^{-1}\text{PCU}^{-1}$	-0.27 ± 0.05	81.3	1.18
Exponential decay ^e	$F_q(10^{-11}\text{ergs s}^{-1}\text{cm}^{-2})$	$F_p(10^{-11}\text{ergs s}^{-1}\text{cm}^{-2})$	τ (days)	χ^2	χ^2/ν
<i>XMM</i> UF (BB+PL) ^b	(1.81 ± 0.01)	(2.97 ± 0.06)	13.3 ± 0.7	5.39	1.08
<i>XMM</i> UF (BB+BB) ^c	(1.62 ± 0.01)	(2.69 ± 0.05)	12.7 ± 0.7	1.737	0.35
<i>RXTE</i> PF ^d	$(0.362 \pm 0.005)\text{cts s}^{-1}\text{PCU}^{-1}$	$(0.46 \pm 0.03)\text{cts s}^{-1}\text{PCU}^{-1}$	134 ± 15	113.5	1.65

^aPower law decay model defined as $F(t) = F_b((t - t_g)/(1 \text{ day}))^\alpha + F_q$, where $F(t)$ is unabsorbed flux, F_q is the quiescent flux, α is the power law index and t_g is the glitch epoch MJD 52,443.13.

^b*XMM* unabsorbed flux decay measured using a blackbody plus power law spectral model.

^c*XMM* unabsorbed flux decay measured using a double-blackbody spectral model.

^d*RXTE* area pulsed flux in units of $\text{cts s}^{-1}\text{PCU}^{-1}$.

^eExponential decay model, defined as $F(t) = F_p e^{-(t-t_g)/\tau} + F_q$, where $F(t)$ is unabsorbed flux, F_p is the peak flux, F_q is the quiescent flux, τ is the decay timescale and t_g is the glitch epoch MJD 52,443.13.

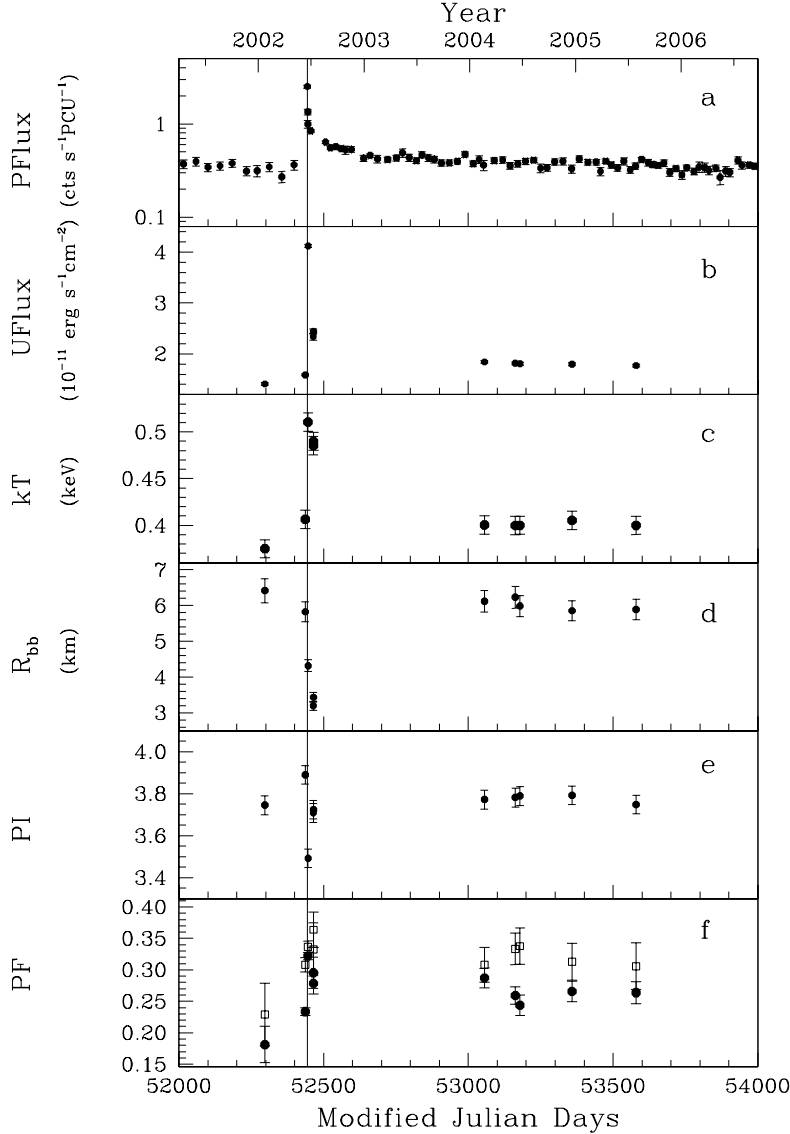


Fig. 1.— Spectral and pulsed fraction evolution of 1E 2259+586 during and following its 2002 outburst. (a) 2–10 keV area pulsed flux measured in *RXTE* monitoring observations; (b) 2–10 keV unabsorbed phase-averaged flux from *XMM* observations (all lower panels are also from *XMM* observations); (c) blackbody temperature (kT), (d) blackbody radius; (e) photon index; (f) 0.1–2 keV area pulsed fraction (*filled circles*) and 2–10 keV area pulsed fraction (*open boxes*). A distance of 3 kpc (Kotthes et al. 2002) is assumed to calculate the blackbody radius. The vertical line denotes the 2002 glitch epoch, MJD 52,443.13 (Woods et al. 2004).

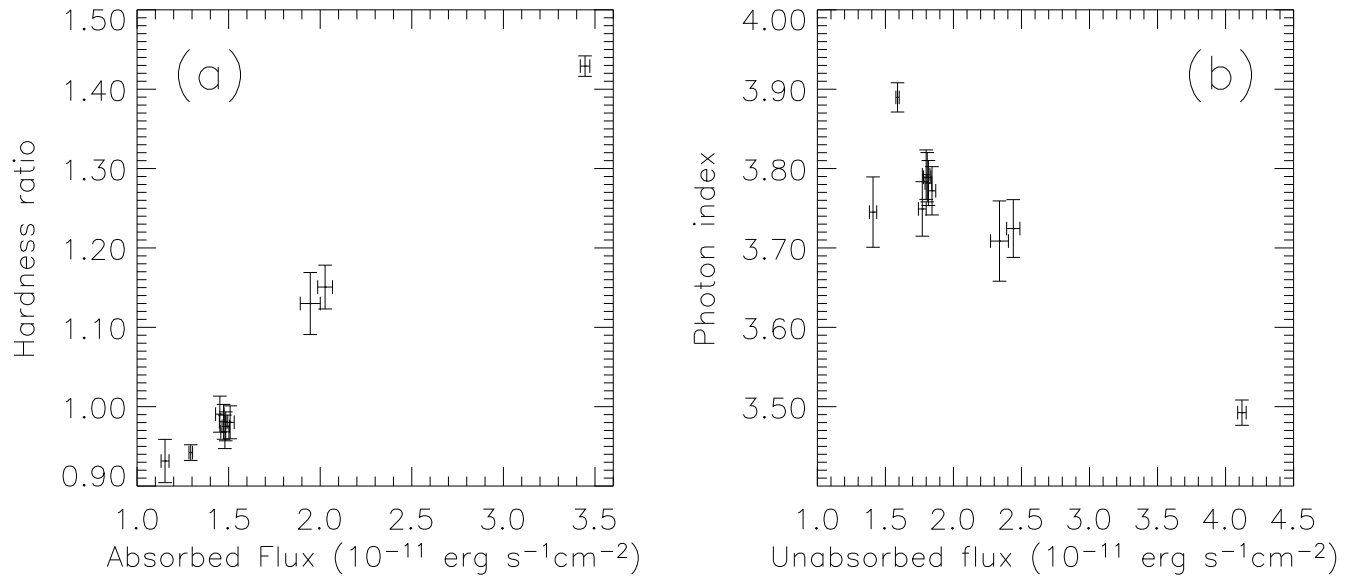


Fig. 2.— (a) Hardness vs. absorbed flux. Hardness ratio is defined as the ratio of 2–10 to 0.1–2 keV absorbed flux. (b) Photon index vs. 2–10 keV unabsorbed flux.

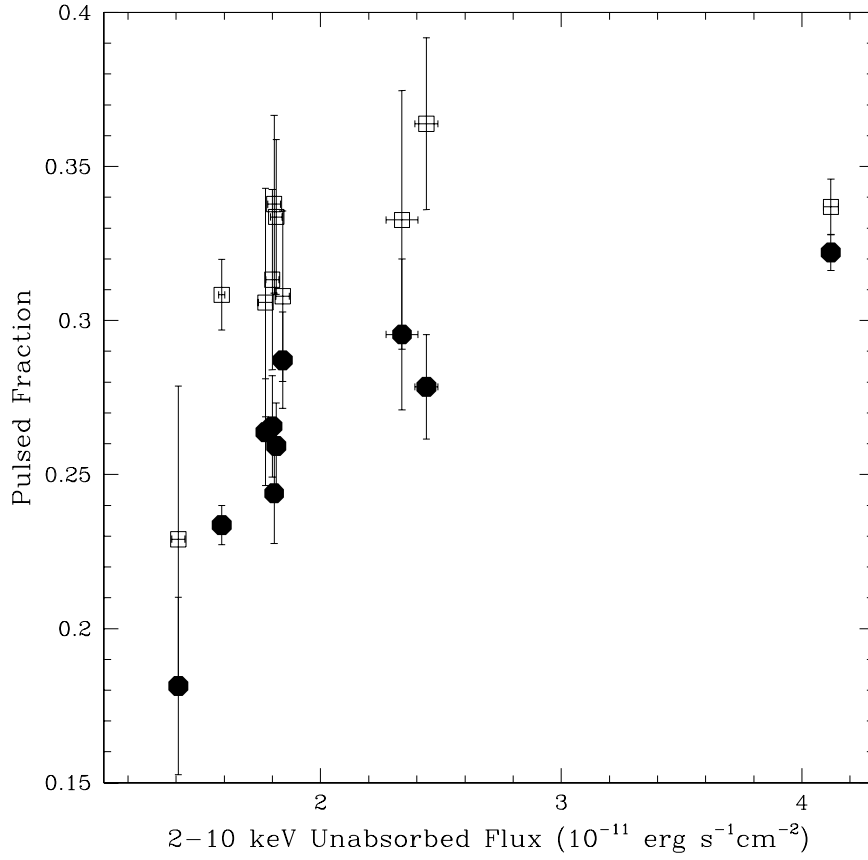


Fig. 3.— The 2–10 keV area pulsed fraction (*open boxes*) vs. 2–10 keV unabsorbed flux ; 0.1–2 keV area pulsed fraction (*filled circles*) vs. 2–10 keV unabsorbed flux.

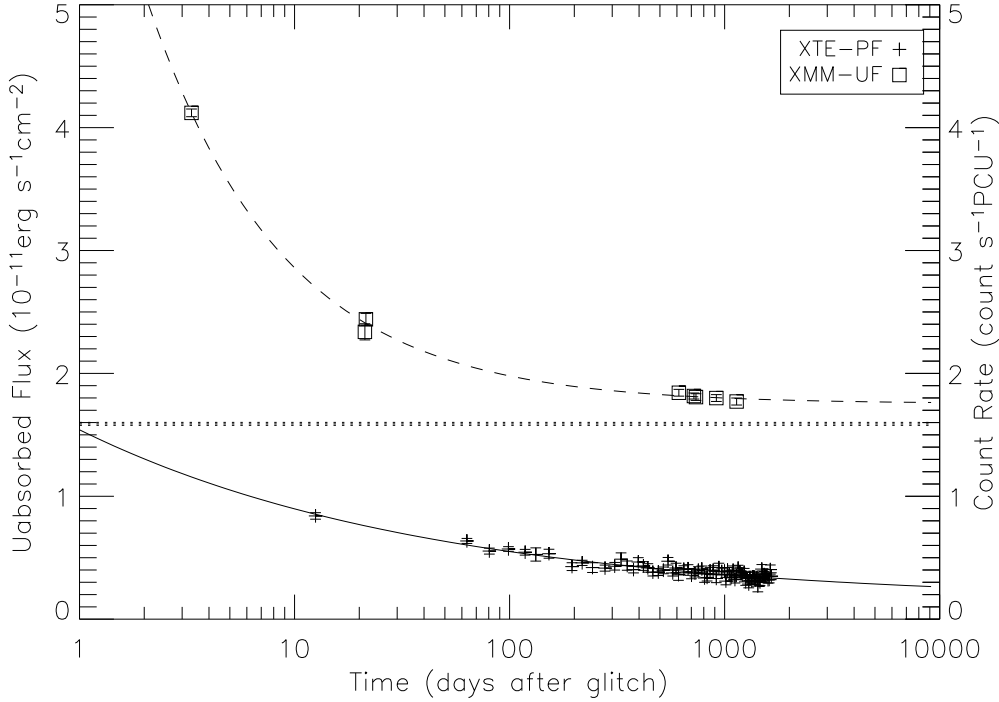


Fig. 4.— Evolution of 1E 2259+586’s 2–10 keV unabsorbed phase-averaged flux (*squares*) measured from *XMM* observations and 2–10 keV area pulsed flux (*cross*) from *RXTE* observations following its 2002 outburst. *XMM* unabsorbed fluxes are in units of 10^{-11} ergs s^{-1} cm $^{-2}$. *RXTE* area pulsed fluxes are in units of count s^{-1} PCU $^{-1}$. The time axis is relative to the estimated glitch epoch (MJD 52,443.13). The solid line is the power law plus constant model fit to the *RXTE* area pulsed fluxes. The dashed line is a fit of the same model, although having different best-fit parameters, to the *XMM* fluxes. See Table 3 for the best-fit parameters. The dotted line is the flux level in 10^{-11} ergs s^{-1} cm $^{-2}$ observed with *XMM* one week before the outburst. The uncertainty on this preoutburst flux is approximately the width of the line.